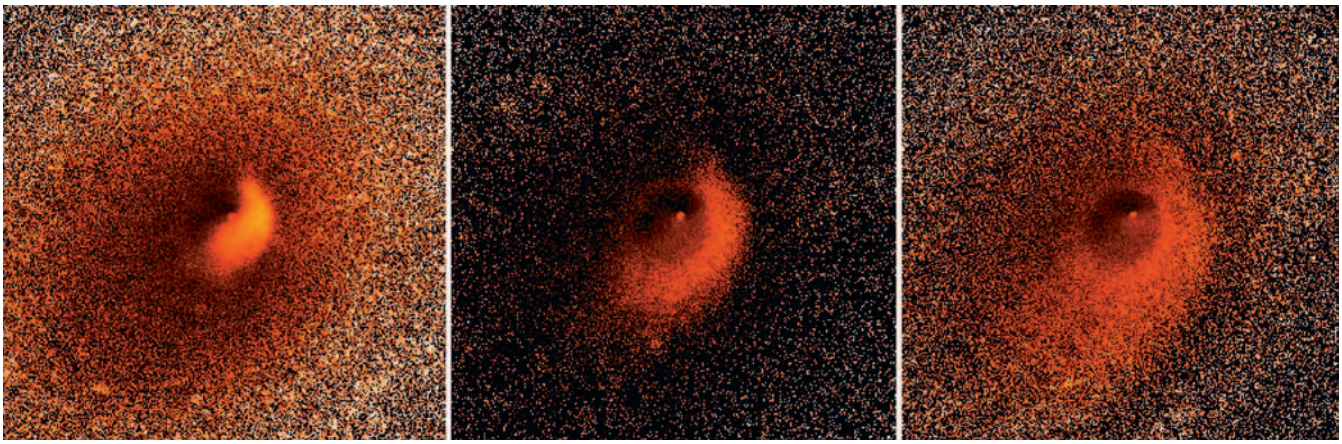

Figure 3. These dramatic images of the expanding and dissipating ejecta plume were obtained by dividing the July 4th, 5th, and 6th coadded images of the comet by the pre-impact image on July 3rd. North is up and East to the left. The plume expands mostly into the South-Western quadrant, and appears to be decelerating at a non-uniform rate. The dust particles at the leading edge of the plume, are expanding at a rate of ~210 m s^{-1} (±10%) on July 4th (measured at a Position Angle of 225°). The field of view in every image is 190×190 arcseconds, which is equivalent to ~123,000×123,000 km at the comet.

Our observing slot ran from July 1st to July 7th, 2005. A period which overlapped the Deep Impact encounter allowing us three nights pre-impact and four nights post impact observing. Our strategy was to use the Wide Field Camera to obtain image mosaics up to 5 million kilometres along the projected anti-solar direction to look for ion-tail features that may have been produced as a result of the impact. The post impact observations quickly revealed that no such ion features were present, which was subsequently confirmed by other observers performing similar programs. With this in mind we decided to focus on deep optical imaging of the central gas and dust coma through *UBVr'i'O+* filters. We were rather fortuitous in that the observing conditions remained beautifully clear for the entire duration of the observing run.

When we imaged the comet on July 4th, about 16 hours after the impact, the comet was seen to have increased in brightness by a factor of two — as measured in the central pixel — compared to the July 3rd pre-impact levels. Some dramatic changes were seen in the dust coma which are shown in Figures 1–3. The Deep Impact event did not create a new period of sustained cometary activity, and in many ways the artificial impact resembled a natural outburst (The Tempel 1 Observing Collaborators Team, 2005; Lara et al., 2005). The observed optical properties of the dust coma from this abundant data set will be modelled by our team. ¤

References:

The Tempel 1 Observing Collaborators Team, 2005, *Science*, **310**, 265.

Lara L. et al., 2005, in preparation.

Stephen Lowry (s.c.lowry@qub.ac.uk)

The SAURON View of the Nuclear Ring in M100

Emma L. Allard[1], Johan H. Knapen[1] and Reynier F. Peletier[2]

1: Centre for Astrophysics Research, University of Hertfordshire; 2: Kapteyn Institute, University of Groningen.

Nuclear rings located within the central 1–2 kiloparsecs of barred spiral galaxies are often found to contain a large fraction of the total star formation taking place in a galaxy (Knapen et al., 2000; Benedict et al., 2002). Under the influence of a bar, gas can be channelled inwards along narrow ridges where shocks develop in the gas flow. We observe these shocks as dark dustlanes along the length of the bar, as can be seen in Figure 1, a real-colour image of the spiral galaxy NGC 4321, perhaps better known as Messier 100. The presence of the bar can set up resonances in the disk. At the location of these resonances, gas experiences no net torque, and hence can accumulate, forming a ring. Through gravitational instabilities or shocks in the gas, star formation can be triggered, and the result is a brightly star-forming nuclear ring, such as we see in M100 (Figure 1). Nuclear rings exist in some 20% of local spiral galaxies (Knapen, 2005). The process of massive star formation in these rings transforms inflowing disk gas into stars, and can thus contribute to the growth of the bulge, assisting the secular evolution of its host galaxy (Kormendy & Kennicutt, 2004).

Most of what is known about the dynamical origin and evolution of these rings stems from detailed numerical modelling, confirmed on the observational side mainly from the gas kinematics. Two-dimensional kinematics of the stars from actual observations are mostly lacking, but

are needed to provide essential constraints on the theoretical models. In addition, detailed spectroscopic studies of the stellar populations in the rings are rare, but needed to confirm the detailed mechanism leading from inflowing gas to star formation.

Observations and Data Reduction

We have observed the nearby spiral galaxy M100 with the SAURON integral field unit (Bacon et al., 2001) on the WHT to help rectify this situation. SAURON boasts a relatively large field of view of 33×41 arcsec, and by using 3 pointings mosaiced together we have covered the ring and bar region of M100 (Figure 1). SAURON has a wavelength range of 4760–5350Å, which contains the Hβ and [OIII] emission lines from which we can measure the gas kinematics, and the Hβ and Mg*b* absorption lines to measure the stellar kinematics.

The data were reduced using the specially developed `XSauron` software (Bacon et al., 2001) and were spatially binned to a constant signal to noise ratios of 10 for the gas and 60 for the stars (using the Voronoi 2D binning method of Cappellari & Copin, 2003). To extract the kinematics, we have made use of the Penalized Pixel Fitting method (PPXF) of Cappellari & Emsellem (2004). This method fits the galactic spectrum to a stellar template library (Vazdekis, 1999) while convolving with a line of sight velocity distribution (LOSVD). We fit the LOSVD with a modified Gaussian and from this we derive the stellar kinematics. With this technique we can successfully separate the stellar and gas components in the individual spectra. To measure the gas kinematics we fit individual Gaussians to the emission lines. Using the PPXF method it is also possible to measure emission and absorption line strengths.

Results

We present here some of the most salient results from our analysis (see also Allard et al., 2005).

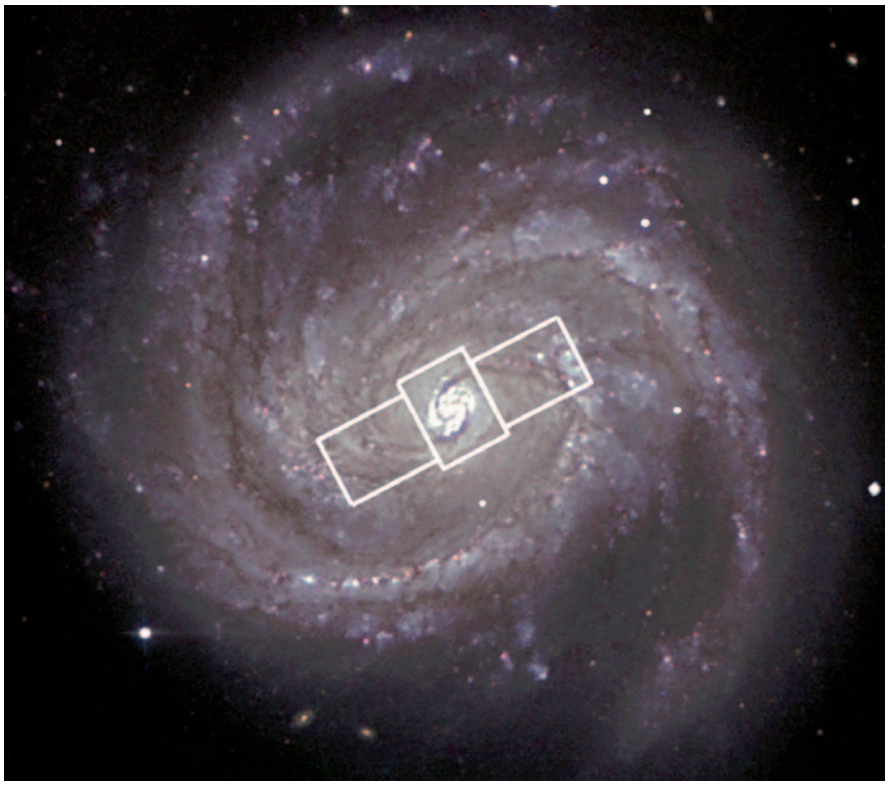

Figure 1. Optical image of M100 (courtesy of Nik Szymanek) showing the location of the three SAURON fields. Our fields span the complete bar, while the nuclear ring is contained within the central pointing. All images shown in this paper are orientated North up, and East to the left. Reproduced with permission from Allard et al. (2005).

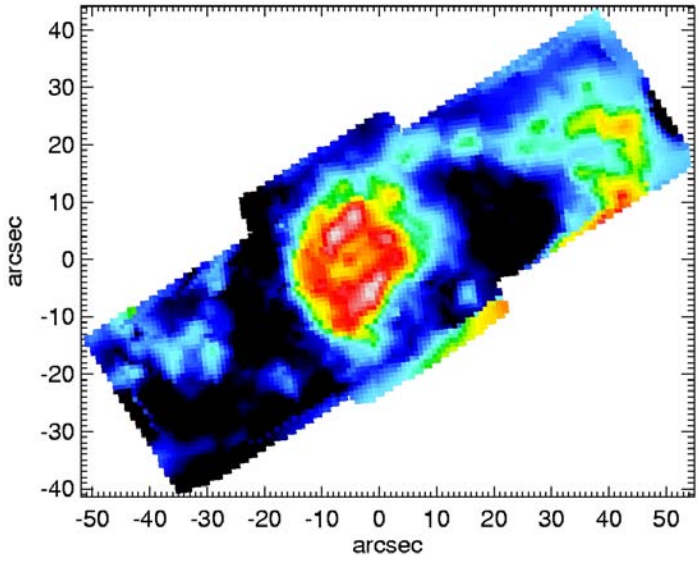

Figure 2. Hβ emission across the field. Reproduced with permission from Allard et al. (2005).

Firstly, we describe the Hβ emission across the field (Figure 2). This shows clearly the nuclear ring of star formation, connected to a cluster of HII regions at the end of the bar (at a position angle of 153°) by a thin arc of emitting material. A closer inspection of the ring reveals it to consist of four tightly wound spiral armlets (cf. Knapen et al., 1995a, b).

The gas and stellar velocity fields are presented in Figures 3 and 4. The stellar kinematics probe the underlying gravitational potential while the gas kinematics probe the response of the gas to this potential. The gas velocity field (Figure 3) shows strong deviations from circular motion, evident from the twists and wiggles in the velocity contours near the centre of the galaxy

(previously seen in the Hα velocity field, Knapen et al., 2000). These deviations are interpreted as a combination of two effects: streaming motions due to a spiral density wave and streaming due to the bar.

The stellar velocity field (Figure 4) shows predominantly circular motion, although some indication of non-circular motions is present along the minor axis of the bar, at the location of the nuclear ring. This may either be due to the stellar orbits being affected by the injection of gas into the region, or to young stars having similar kinematics to their parent gas cloud. As our stellar kinematics are derived from stellar absorption features, strongest in older stars, the former explanation is more plausible.

Relatively Cool Gas from which Stars Form

We also present here the gas velocity dispersion across the field (Figure 5). This shows a high central value of around 130 km/s, and a much lower value of around 60 km/s in a ring around the centre. We have overlaid Hβ emission contours over the dispersion map to show that this low dispersion material lies at the exact location of the star forming ring. The low gas dispersion at the location of the ring is further evidence of the existence of a resonance region there, specifically the pair of Inner Lindblad resonances described before (e.g., Knapen et al., 1995a). Cold gas is very unstable to star formation, and we are detecting here the cold gas from which the massive stars form.

The relatively low dispersion gas is also spatially correlated with Hβ emission at other locations, such as in the HII regions at the end of the bar and along the thin arc connecting these with the ring. This confirms that the origin of the cold gas is further out in the disk of the galaxy, and that it is being driven inwards along the dustlanes in the bar, where it finally accumulates in a ring (Allard et al., 2005).

The Hβ emission appears to follow the curved dustlanes, as can be seen in

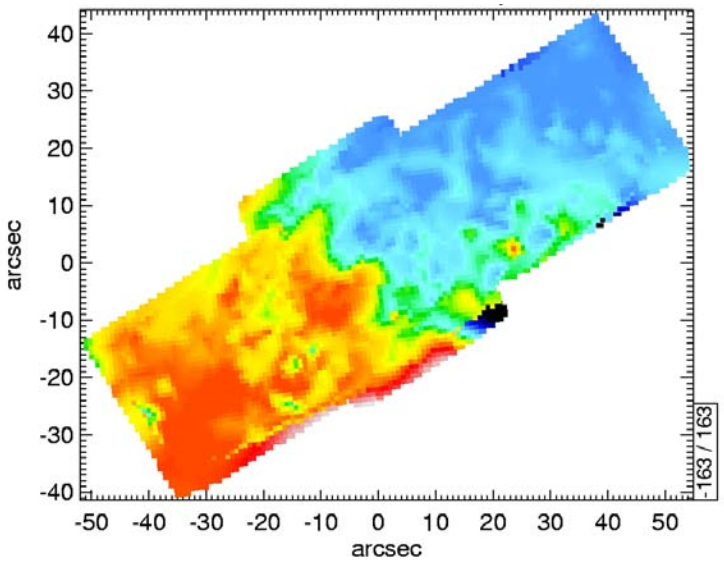

Figure 3. Mean gas velocity field. Red and blue indicate redshifted and blueshifted material. The minimum and maximum values are quoted in the bottom right box.

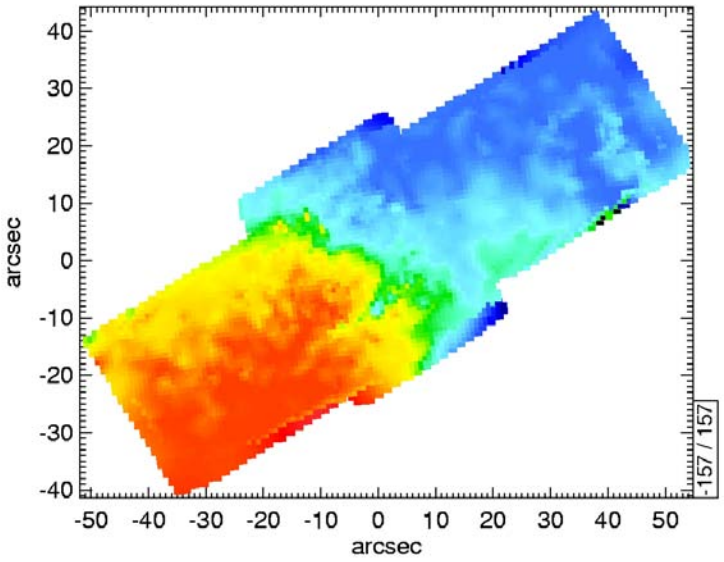

Figure 4. As Figure 3, now for the mean stellar velocity field.

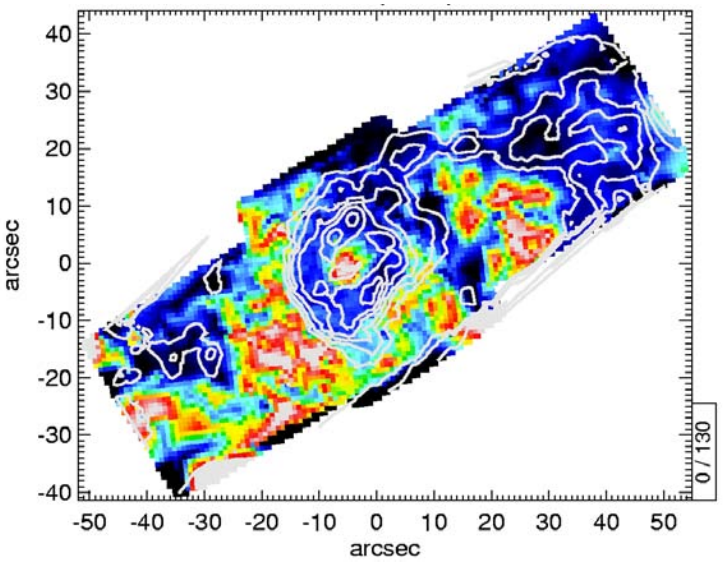

Figure 5. Gas velocity dispersion across the field. Overlaid are Hβ emission contours indicating the location of the ring. Values are in km/s with red and blue colours representing high and low values respectively. Reproduced with permission from Allard et al. (2005).

Figure 1, so to investigate any spatial correlation between the two we have overlaid Hβ emission contours onto a *B*–*R* colour image (Figure 6). There is a clear offset between the dustlanes and the star formation of around 700 pc. At the location of the shocks we expect strong shear, and so star formation will be prevented. Immediately downstream from the shock, however, the piling up of gas allows material to cool and acquire lower velocity dispersion, and star formation can be triggered.

Summary

The results presented here support the theoretical picture in which star formation at the centres of spiral galaxies is brought about by the injection of gas into the area through shocks (manifested as dustlanes), and the creation of rings in the presence of resonances. Our SAURON data have allowed an unprecedented view of the two-dimensional relationships between the different gas and stellar tracers. Further results from our analysis will be published in a forthcoming paper (Allard, Knapen & Peletier, in preparation). ¤

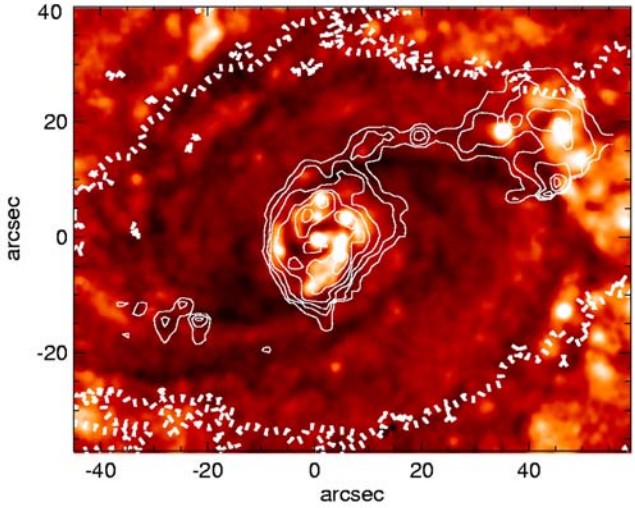

Figure 6. B–R image of M100. Overlaid are Hβ emission contours (thin white line), and a K_S-band contour outlining the bar (white dashed line). Reproduced with permission from Allard et al. (2005).

References:

Allard, E. L., Peletier, R. F., Knapen, J. H., 2005, *ApJ*, **633**, L25.

Bacon, R., et al., 2001, *MNRAS*, **326**, 23.

Benedict, G. F., Howell, D. A., Jørgensen, I., Kenney, J. D. P., Smith, B. J., 2002, *AJ*, **123**, 1411.

Cappellari, M., Copin, Y., 2003, *MNRAS*, **342**, 345.

Cappellari, M., Emsellem, E., 2004, *PASP*, **116**, 138.

Knapen, J. H., 2005, *A&A*, **429**, 141.

Knapen, J. H., Beckman, J. E., Heller, C. H., Shlosman, I., de Jong, R. S., 1995a, *ApJ*, **454**, 623.

Knapen, J. H., Beckman, J. E., Shlosman, I., Peletier, R. F., Heller, C. H., de Jong, R. S., 1995b, *ApJ*, **443**, L73.

Knapen, J. H., Shlosman, I., Heller, C. H., Rand, R. J., Beckman, J. E., Rozas, M., 2000, *ApJ*, **528**, 219.

Kormendy, J., Kennicutt, R. C., 2004, *ARA&A*, **42**, 603.

Vazdekis, A., 1999, *ApJ*, **513**, 224.

Emma Allard (allard@star.herts.ac.uk)

TELESCOPES AND INSTRUMENTATION

Progress on the GLAS Rayleigh Laser Beacon System for the William Herschel Telescope

René G. M. Rutten (ING) and Gordon Talbot (ING)

Adaptive Optics (AO) has been central to the development strategy of the WHT. The generally good seeing conditions make the site very attractive for AO exploitation and has the potential to offer major new advantages for astronomy. The higher spatial resolution achieved through AO has the obvious advantage of distinguishing finer structure and avoiding source confusion in dense fields.

Existing AO instrumentation at the WHT, NAOMI, is located in a purpose built enclosure occupying one of the Nasmyth foci. Science instruments include a 1024 by 1024 pixel HgCdTl infra-red camera, INGRID, an optical integral field spectrograph, OASIS, and a coronagraph unit, OSCA. In particular the OASIS spectrograph offers unique capability, and for that reason the focus of AO science exploitation lies in the wavelength range of 0.6 to 1.0 micron.

Although natural guide star operation of the NAOMI AO system is now well established, the limited sky coverage for higher order AO operation has proven a serious limiting factor in its science use. For that reason in 2004 a project was embarked upon to develop a facility class general purpose Rayleigh laser beacon system. The